

Quantum error correction for long chains of trapped ions

Min Ye and Nicolas Delfosse

IonQ Inc.

(Dated: March 31, 2025)

We propose a model for quantum computing with long chains of trapped ions and we design quantum error correction schemes for this model. The main components of a quantum error correction scheme are the quantum code and a quantum circuit called the syndrome extraction circuit, which is executed to perform error correction with this code. In this work, we design syndrome extraction circuits tailored to our ion chain model, a syndrome extraction tuning protocol to optimize these circuits, and we construct new quantum codes that outperform the state-of-the-art for chains of about 50 qubits. To establish a baseline under the ion chain model, we simulate the performance of surface codes and bivariate bicycle (BB) codes equipped with our optimized syndrome extraction circuits. Then, we propose a new variant of BB codes defined by weight-five measurements, that we refer to as BB5 codes, and we identify BB5 codes that achieve a better minimum distance than any BB codes with the same number of logical qubits and data qubits, such as $[[30, 4, 5]]$ and $[[48, 4, 7]]$ BB5 codes. For a physical error rate of 10^{-3} , the $[[48, 4, 7]]$ BB5 code achieves a logical error rate per logical qubit of $5 \cdot 10^{-5}$, which is four times smaller than the best BB code in our baseline family. It also achieves the same logical error rate per logical qubit as the distance-7 surface code but using four times fewer physical qubits per logical qubit.

I. INTRODUCTION

Fault-tolerant quantum computing relies on extensive quantum error correction to correct faults occurring during the computation before they spread to all the qubits. To maximally benefit from quantum error correction, it is crucial to design quantum error correction schemes that are tailored to the specific constraints of the hardware. Surface codes [1, 2] and color codes [3], which are defined by local measurements on a lattice of qubits, naturally fit with superconducting chips, consisting of a square grid of qubits with nearest neighbor connectivity [4–9]. Quantum error correction schemes have been optimized for several other hardware platforms such as Majorana qubits [10, 11], neutral atoms [12–16], cat qubits [17–19], photonic qubits [20–23] or short ion chains with shuttling [24–26].

In this work, we investigate the question of designing quantum error correction schemes for a long chain of trapped ions, which is the core module of a trapped ion quantum computer. The potential of long ion chains has been demonstrated experimentally over the past 10 years with 5-ion chains running Shor’s algorithm [27] or Deutsch–Jozsa and Bernstein–Vazirani algorithms [28], a 14-ion GHZ state [29], a quantum chemistry algorithm executed on a 15-ion chain [30], and quantum error correction experiments with chains of 13 to 16 ions [31–33]. The performance of a 30-qubit quantum computer based on a long chain of ions is analyzed in [34]. Chains with more than 50 ions have been used for analog quantum simulations [35, 36]. The loading of a chain of 155 ions is reported in [37]. Architectures for large-scale quantum computers based on ion chains connected through shuttling or optical interconnects are proposed in [38–40]. For a review of trapped ion quantum computing see [41].

The major advantages of long ion chains is their large coherence time and high connectivity. Current

trapped ion technologies achieve a gate error rate close to 10^{-3} for two-qubit gates and 10^{-4} for single-qubit gates [31, 34, 42, 43]. Moreover, qubits stored in a long ion chain are fully connected, in the sense that the native gate set includes entangling gates for every pair of qubits [44, 45]. This high connectivity suggests that trapped ions could be a good fit for the implementation of quantum low-density parity-check (LDPC) codes. Recent simulations show that quantum LDPC codes achieve a significantly lower overhead than surface codes while maintaining the same logical error rate [46–48]. However, these codes require some form of long-range connectivity that is not available in today’s superconducting chips. This makes long ion chains a natural candidate to host quantum LDPC codes, but a detailed analysis is needed to confirm this intuition. There are major differences between the model considered in previous simulations of quantum LDPC codes and the capability of trapped ion qubits. These differences could translate to a large gap between simulation results and a real implementation of these codes.

To close this gap, we propose the *ion chain model*, which captures the main features of quantum computing with a long ion chain. Namely, (i) idle qubits have very long coherence time, (ii) two-qubit operations are noisier than single-qubit operations, which are noisier than idle qubits, (iii) qubits are fully connected, (iv) unitary gates are sequential: One can only implement a single unitary gate at a time, (v) reset and measurement are parallel: One can reset or measure any subset of qubits in parallel, (vi) measurements are slower than other operations. Property (i) and (iii) suggest that quantum LDPC codes should be a good fit for such a quantum platform. However, one could be concerned that (iv) and (vi) may result in a significant degradation of the code performance, making quantum LDPC codes unsuitable for this model, and these limitations are not reflected in the quantum

LDPC code simulations cited above.

We study the performance of quantum error correction codes encoding k logical qubits into n data qubits with $n \leq 50$. Including ancilla qubits, all the quantum error correction schemes designed in this paper use a chain of at most 57 qubits. The code parameters are denoted $[[n, k]]$, or $[[n, k, d]]$ if the minimum distance d is known, and the number of ancilla qubits is denoted n_a . The minimum distance d measures the error correction capability of the code.

Quantum error correction is implemented by executing a quantum circuit called the syndrome extraction circuit. We design syndrome extraction circuits respecting the constraints of the ion chain model (Algorithm 1), that can be used for any stabilizer codes [49]. The high connectivity of the ion chain model offers a lot of flexibility in the construction of this circuit. To exploit this freedom, we propose a syndrome extraction tuning protocol (Algorithm 2) that optimizes the syndrome extraction circuit to achieve a favorable tradeoff between logical error rate and qubit overhead.

To establish a baseline for the ion chain model, we consider surface codes, which achieve state-of-the-art performance for superconducting architecture [1, 2], and bivariate bicycle (BB) codes, which achieve state-of-art performance when long-range gates are available [47]. We simulate the performance of these codes with a syndrome extraction circuit optimized for the ion chain model. Our baseline family includes surface codes with distance 3, 5 and 7. The number of BB codes with up to 50 data qubits is massive and some of them have poor parameters. Therefore, we do not simulate all of them. Instead, we simulate a BB code with optimal minimum distance d for each achievable pair of $[[n, k]]$ within the BB code family for $n \leq 50$.

Finally, we propose a new variant of BB codes defined by weight-5 stabilizer generators, in contrast to the weight-6 stabilizer generators of the original BB codes. We refer to these new codes as BB5 codes. To avoid any confusion, in the rest of this paper we use the term BB6 codes for the original BB codes of [47]. We identify two BB5 codes with parameters $[[30, 4, 5]]$ and $[[48, 4, 7]]$ that achieve larger code distance than any BB6 code with the same parameters $[[n, k]]$. For comparison BB6 codes only achieve $[[30, 4, 4]]$ and $[[48, 4, 6]]$. Our simulations show that, under the ion chain model, the $[[48, 4, 7]]$ BB5 code achieves a logical error rate per logical qubit 4 times smaller than the best BB6 codes with code length up to 50. Moreover, it reaches the same logical error rate per logical qubit as the distance-7 surface code while using 4 times fewer physical qubits per logical qubit.

The rest of this paper is organized as follows. Section II introduces the ion chain model. Syndrome extraction circuits for the ion chain model are designed and optimized in Section III. In Section IV, we investigate the performance of surface codes and BB codes under the ion chain model and we design new codes that outperform these codes.

II. THE ION CHAIN MODEL

The ion chain model describes the connectivity, the parallelism and the noise rate of quantum operations in a chain of trapped ions. It is a useful model for machines such as the IonQ Forte system and the ion chain experiments cited in introduction. The ion chain model, denoted **Chain**(n, p, τ_m), has three parameters: n for the number of qubits, p for the noise parameter and τ_m which controls the measurement time. We refer to a register of qubits for this model as a n -qubit chain and p is called the *physical error rate*. This section describes the properties of n -qubit chains.

A n -qubit chain is a register of n qubits equipped with the following operations: (i) prepare or reset any subset of qubits in the state $|0\rangle$, (ii) apply a single-qubit unitary gate to any qubit, (iii) apply a two-qubit unitary gate to any pair of qubits, (iv) measure any subset of qubits in the computational basis. We assume that these operations are applied sequentially, *i.e.* only one of these operations can be executed at a given time step.

We adopt the standard circuit level noise model in which every operation is followed by depolarizing noise. A two-qubit unitary gate is followed by a random two-qubit Pauli error with probability p . This error is selected uniformly among the 15 Pauli errors acting non-trivially on the support of the gate. A single-qubit operation (preparation, reset or unitary gate) is followed by a random single-qubit Pauli error with probability $p/10$. This error is selected uniformly among X, Y , and Z errors. The outcome of a measurement is flipped with probability $p/10$. During a gate, any idle qubit suffers from a random single-qubit Pauli error with probability $p/100$.

Finally, we assume that all the operations have the same duration, except measurements which take τ_m times longer. This long measurement time translates to more idle noise during a measurement. We consider a regime with $\tau_m p \ll 100$ and we set the idling noise rate during a measurement to $\tau_m p/100$. In our simulations, we use $\tau_m \approx 30$.

In practice, the ions are confined by an electromagnetic field. Each qubit is stored within two energy levels of an ion. A n -qubit chain may contain more than n ions if we use additional ions for sympathetic cooling [50]. Remarkably, operations entangling any of the $\binom{n}{2}$ pairs of qubits are available as native gates in the ion chain model. These operations can be implemented using the Mølmer-Sørensen scheme by illuminating the targeted ions using two laser beams [44, 45]. This allows us to operate on a pair of distant qubits by controlling the laser beams without moving the ions. The operation is mediated by the common vibrations of the ions. See Fig. 1 of [34] for an illustration and for more details on the experimental setup.

III. SYNDROME EXTRACTION CIRCUITS FOR THE ION CHAIN MODEL

We focus on *stabilizer codes* which are defined as the common +1-eigenspace of a family of commuting Pauli operators called *stabilizer generators* [49].

The *syndrome extraction circuit* is the quantum circuit that performs the measurement of the stabilizer generators of the code. It is executed periodically to correct errors. The ion chain model offers a lot of flexibility when designing syndrome extraction circuits, which can be used to reduce the qubit overhead of quantum error correction. For instance, the all-to-all qubit connectivity enables the use of a single ancilla qubit to sequentially measure all stabilizer generators for any code. This reduces the qubit overhead of the surface and BB6 codes by a factor of almost 2. Note that this is not possible for quantum hardware with local connectivity constraints, where a single ancilla qubit can only measure stabilizers supported on its neighbors. On the other hand, using a single ancilla qubit may result in a long waiting time and a suboptimal logical error rate. To speed up the syndrome extraction and to reduce the logical error rate, one may use multiple ancilla qubits that are measured simultaneously. In this section, we design a family of syndrome extraction circuits with a variable number of ancilla qubits. Then, we propose a protocol to select the number of ancilla qubits that optimizes the tradeoff between the qubit overhead and the logical error rate.

Algorithm 1: Ion chain syndrome extraction circuit

Input: A list of n -qubit Pauli operators S_0, S_1, \dots, S_{r-1} supported on qubits $0, 1, \dots, n-1$. An integer $n_a \geq 1$.

Output: A quantum circuit measuring the operators S_0, S_1, \dots, S_{r-1} .

```

1 for  $i = 0, 1, \dots, \left\lceil \frac{r}{n_a} \right\rceil - 1$  do
2   for  $j = 0, 1, \dots, n_a - 1$  do
3      $k \leftarrow in_a + j$ .
4      $c \leftarrow n + j$ .
5     Prepare qubit  $c$  in the state  $|0\rangle$ .
6     Apply a  $H$  gate to qubit  $c$ .
7     for  $t = 0, 1, \dots, n-1$  do
8       if the component  $P$  of  $S_k$  on qubit  $t$  is
           $P = X, Y$  or  $Z$  then
9         Apply a controlled- $P$  gate controlled
            on qubit  $c$  with target qubit  $t$ .
10    Apply a  $H$  gate to qubit  $c$ .
11    if  $k \geq r-1$  then break;
12    Measure qubits  $n, n+1, \dots, n+j$ .
```

The *ion chain syndrome extraction circuit* is described in Algorithm 1. This circuit fits the constraints of the ion chain model. It measures Pauli operators supported on n data qubits indexed by $0, 1, \dots, n-1$ using n_a ancilla qubits indexed by $n, n+1, \dots, n+n_a-1$. The ancilla qubits are measured simultaneously. The parallelization

of these measurements yields a significant reduction of the total idle time of the qubits because measurements are the slowest operations in the ion chain model. Other gates remain sequential to respect the ion chain model.

To obtain the syndrome extraction circuit of a stabilizer code with r rounds of syndrome extraction, we set the input of Algorithm 1 as the stabilizer generators of the code repeated r times. In numerical simulations, we use $r = d$ rounds of syndrome extraction where d is the minimum distance of the code, which is a standard choice in the literature. Algorithm 1 is used with an input sequence alternating X and Z operators.

To optimize the syndrome extraction circuit, we need to identify a sweet spot between the number of ancilla qubits consumed and the logical error rate achieved. We propose the *syndrome extraction tuning protocol* described in Algorithm 2. The protocol keeps increasing the number n_a of ancilla qubits as long as each iteration reduces the logical error rate by a factor γ . The optimized number of ancilla qubits n_a returned by Algorithm 2 depends on the code, the measurement time τ_m , and to a lesser extent on p .

Algorithm 2: Syndrome extraction tuning protocol

Input: A stabilizer code C with n data qubits.

Parameters $p \in [0, 1]$, $\tau_m \in \mathbb{R}_+$ and

$\gamma \in [0, 1]$.

Output: A positive integer n_a .

```

1 Initialize  $n_a = 1$  and  $p_{\log}(0) = 1$ .
2 Estimate the logical error rate  $p_{\log}(n_a)$  of  $C$  with
   the ion chain syndrome extraction circuit using
    $n_a$  ancilla qubits for the model
   Chain( $n + n_a, p, \tau_m$ ).
3 while  $\frac{p_{\log}(n_a)}{p_{\log}(n_a-1)} < \gamma$  do
4    $n_a \leftarrow n_a + 1$ .
5   Estimate the logical error rate  $p_{\log}(n_a)$  of  $C$ 
     with the ion chain syndrome extraction
     circuit using  $n_a$  ancilla qubits for the model
     Chain( $n + n_a, p, \tau_m$ ).
6 return  $n_a$ .
```

IV. IMPROVED CODES FOR THE ION CHAIN MODEL

As a baseline, we consider surface codes [1, 2], and BB6 codes [47]. These code constructions are reviewed in Appendix A. For our baseline family, we select surface codes with minimum distance 3, 5 and 7 and we select a BB6 code achieving the largest minimum distance d for each achievable pair $[[n, k]]$ within BB6 code family for $n \leq 50$. We eliminate codes with $d \leq 2$. The parameters obtained are listed in Table I.

Next we propose a new code family that we call BB5 codes and we show that they outperform all the baseline codes under the ion chain model. Let Q_ℓ be the $\ell \times \ell$ circulant matrix whose first row is $(010\dots 0)$. A BB5

code	parameters	stabilizer weight	optimized n_a
Surface code	[[9, 1, 3]]	≤ 4	4
Surface code	[[25, 1, 5]]	≤ 4	5
Surface code	[[49, 1, 7]]	≤ 4	8
BB6 code	[[18, 4, 4]]	6	4
BB6 code	[[24, 4, 4]]	6	3
BB6 code	[[28, 6, 4]]	6	5
BB6 code	[[30, 4, 4]]	6	3
BB6 code	[[30, 8, 4]]	6	5
BB6 code	[[36, 4, 4]]	6	4
BB6 code	[[36, 8, 4]]	6	4
BB6 code	[[42, 4, 6]]	6	5
BB6 code	[[42, 6, 6]]	6	7
BB6 code	[[48, 4, 6]]	6	6
BB6 code	[[48, 8, 4]]	6	4
BB5 code	[[30, 4, 5]]	5	5
BB5 code	[[48, 4, 7]]	5	6

TABLE I. Parameters of baseline codes and BB5 codes. The optimized n_a is the number of ancilla qubits used for syndrome extraction, selected by Algorithm 2 with parameters $p = 5 \times 10^{-4}$, $\tau_m = 30$ and $\gamma = 0.9$.

$[[n, k, d]]$	ℓ	m	A_1	A_2	A_3	A_4	A_5
[[30, 4, 5]]	5	3	I_{15}	$Q_5 \otimes I_3$	I_{15}	$I_5 \otimes Q_3$	$Q_5^2 \otimes Q_3^2$
[[48, 4, 7]]	8	3	I_{24}	$Q_8 \otimes I_3$	I_{24}	$I_8 \otimes Q_3$	$Q_8^3 \otimes Q_3^2$

TABLE II. Examples of BB5 codes.

code is a CSS code defined by the pair of matrices

$$\mathbf{H}_X = [A_1 + A_2 \mid A_3 + A_4 + A_5],$$

$$\mathbf{H}_Z = [A_3^T + A_4^T + A_5^T \mid A_1^T + A_2^T].$$

Rows of \mathbf{H}_X and \mathbf{H}_Z are respectively the indicator vectors of the X and Z stabilizer generators of the codes [51, 52]. Each A_i is an $(m\ell) \times (m\ell)$ permutation matrix of the form $Q_\ell^u \otimes Q_m^v$ with $u \in \{0, 1, \dots, \ell - 1\}$ and $v \in \{0, 1, \dots, m - 1\}$. Each BB5 code is specified by the values of ℓ, m and the matrices A_1, \dots, A_5 . Table II presents two instances of BB5 codes, found by exhaustive search, achieving a larger minimum distance than any BB6 codes with the same parameter $[[n, k]]$.

To compare BB5 codes against our baseline codes, we estimate their *logical error rate*. In this paper, when we talk about the logical error rate, we always mean the logical error rate per syndrome extraction round and per logical qubit. It is defined as $\frac{q_X + q_Z}{kd}$ where k is the number of logical qubits and d is minimum distance of the code. The value q_Z is defined to be the probability that a Z logical measurement returns a non-trivial outcome in the circuit that initializes all data qubits in the $|0\rangle$ state, performs d rounds of syndrome extraction, measures all the data qubits and extracts the logical outcomes using a decoder. The term q_X is defined analogously for X logical measurements, by inserting H gates on the data

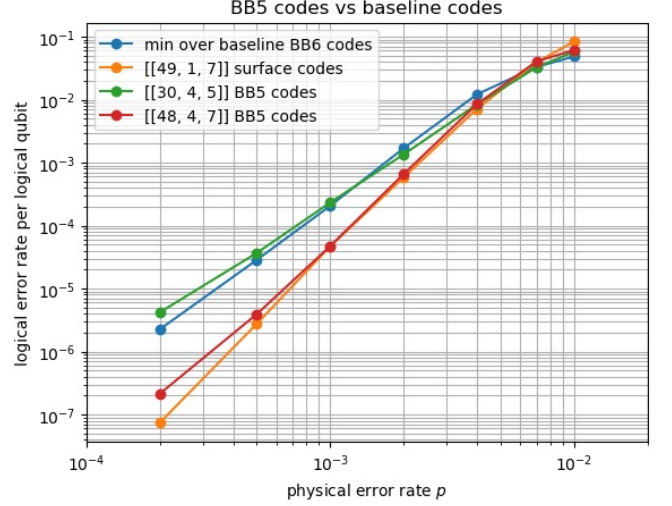


FIG. 1. Comparison between BB5 codes and baseline codes. Each point on the blue curve is the minimum logical error rate per logical qubit for a BB6 code from the baseline family.

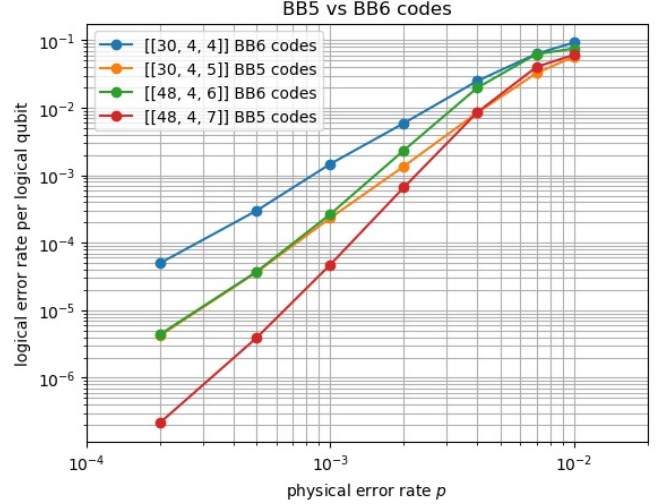


FIG. 2. Comparison between BB5 codes and BB6 codes with the same parameters.

qubits after initialization and before the final measurement. We use the ion chain syndrome extraction circuit of Algorithm 1. The number of ancilla qubits n_a is optimized by Algorithm 2 and reported in Table I.

The logical error rate is estimated with a Monte Carlo simulation using Stim [53], the BP-OSD decoder [54–56] for BB5 and BB6 codes, and PyMatching 2 [57] for surface codes. For all the simulations in this paper, the relative error bar is smaller than 6%.

Fig. 1 shows that the $[[48, 4, 7]]$ BB5 code outperforms all the BB6 codes of our baseline. While the $[[49, 1, 7]]$ surface code exhibits a lower logical error rate per logical qubit at low physical error rates, it encodes 4 times fewer logical qubits than the $[[48, 4, 7]]$ BB5 code. In-

cluding ancilla qubits, the $[[49, 1, 7]]$ surface code uses a total of 57 qubits and the $[[48, 4, 7]]$ BB5 code uses a total of 54 qubits. Fig. 2 compares BB5 and BB6 codes with identical $[[n, k]]$ parameters. For both the $[[30, 4]]$ and $[[48, 4]]$ cases, BB5 codes achieve roughly $6\times$ smaller logical error rate than BB6 codes at physical error rate 10^{-3} . The gap becomes even larger for smaller physical error rates.

V. CONCLUSION

This paper demonstrates that quantum LDPC codes are well suited for long chain of trapped ions and introduces new quantum LDPC codes that outperform state-of-the-art quantum error correction codes.

Moreover, the high connectivity of ion chains allows us to use fewer ancilla qubits than a superconducting implementation, reducing the qubit overhead, at the price of an increased syndrome extraction time due to less parallelism.

The codes, circuits and optimizations proposed in this work may find applications to other platforms beyond long chains of trapped ions, although our ion chain model does not capture some of the features of these platforms, which may affect the performance of the quantum error correction schemes.

In future work, it would be interesting to explore the performance of other classes of small quantum LPDC codes [58–63] under the ion chain model.

VI. ACKNOWLEDGMENTS

We thank John Gamble, Edwin Tham, Neal Pimenti, Laird Egan, Ricardo Viteri, Alex Ratcliffe, Matthew Boguslawski and Dean Kassmann for insightful discussions during the preparation of this manuscript.

Appendix A: Review of surface codes and BB codes

The section reviews the definition of the surface code and BB codes.

The distance- d surface code is a $[[d^2, 1, d]]$ stabilizer code defined on a $d \times d$ two-colored square tiling as shown in Fig. 3. Qubits are placed on the d^2 vertices and each tile defines a stabilizer generator acting on the four incident qubits either as X or Z depending on the tile color. The stabilizer generators associated with boundary tiles act on two qubits only.

To introduce BB6 codes, we define the matrices $x = Q_\ell \otimes I_m$ and $y = I_\ell \otimes Q_m$ where m and ℓ are two positive integers. A BB6 code is defined by the pair of matrices

$$\begin{aligned} \mathbf{H}_X &= [A_1 + A_2 + A_3 \mid A_4 + A_5 + A_6], \\ \mathbf{H}_Z &= [A_4^T + A_5^T + A_6^T \mid A_1^T + A_2^T + A_3^T], \end{aligned}$$

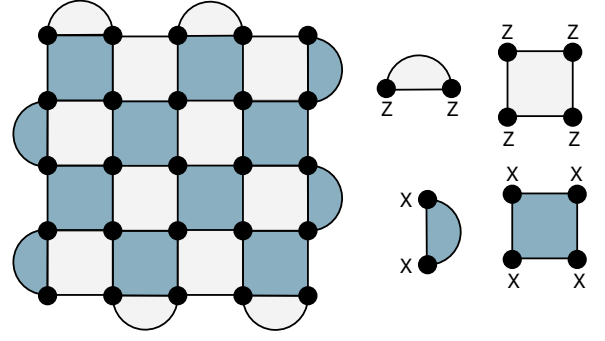


FIG. 3. A distance-5 surface code and its stabilizer generators.

where every A_i is a power of either x or y . Both \mathbf{H}_X and \mathbf{H}_Z have size $(n/2) \times n$. The columns of \mathbf{H}_X and \mathbf{H}_Z correspond to the $n = 2m\ell$ data qubits of the code. Each row of \mathbf{H}_X (respectively \mathbf{H}_Z) is the indicator vector of a X (respectively Z) stabilizer of the code. By specifying m, ℓ and the matrices A_1, A_2, \dots, A_6 , we obtain a BB6 code instance. Given ℓ and m , there are $(\ell + m)^6$ possible BB6 codes.

Appendix B: Validation of the syndrome extraction tuning protocol

To validate the effectiveness of the syndrome extraction tuning protocol described in Algorithm 2, we execute this protocol to optimize the number of ancilla qubits n_a of two BB6 codes with parameters $[[30, 4, 4]]$ and $[[48, 4, 6]]$ and we check that it provides a sensible choice.

To confirm that, we estimate the logical error rate of the two codes across a range of ancilla numbers $n_a = 1, 2, 3, 4, 5, 10, 20$ as shown in Fig. 4. Algorithm 2 selects $n_a = 3$ for the $[[30, 4, 4]]$ BB6 code and $n_a = 6$ for the $[[48, 4, 6]]$ BB6 code. Fig. 4 clearly illustrates that increasing n_a beyond these chosen values provides progressively smaller reductions in logical error rates, indicating diminishing returns. Specifically, for the $[[30, 4, 4]]$ BB6 code, using $n_a = 20$ actually degrades the logical error rate compared to the protocol's selection of $n_a = 3$.

Appendix C: Fitting formulas for surface codes and BB5 codes

Most of the code simulations in previous papers employ a circuit model with parallel gate operations and uniform noise rates [2, 46–48]. We will refer to such a circuit model as the parallel circuit model. Fitting formulas for logical error rates of important code families such as surface codes and BB6 codes were studied under the parallel circuit model [2, 47, 64]. For surface codes,

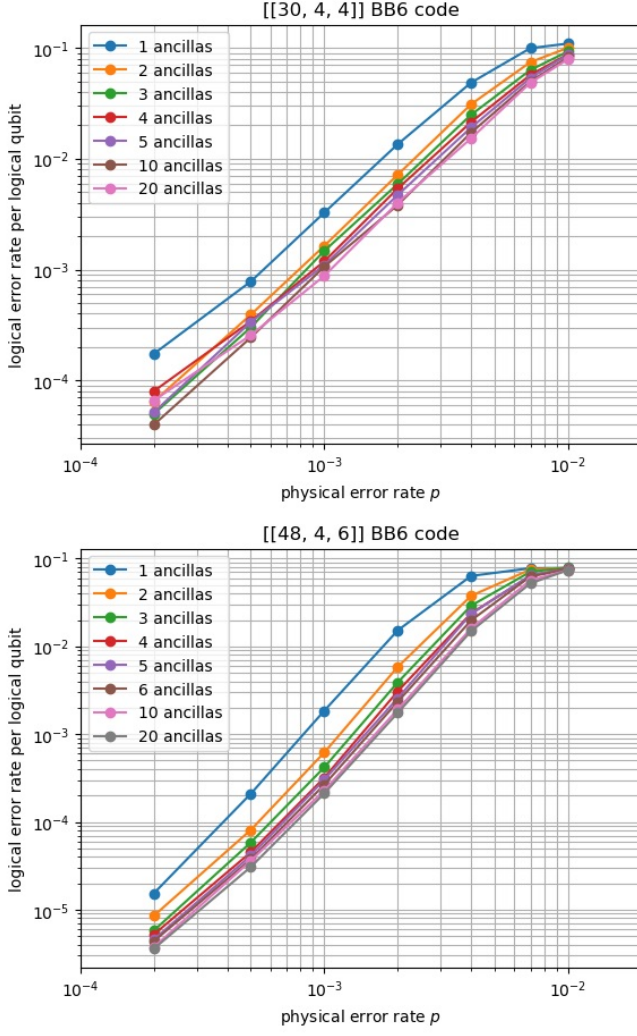


FIG. 4. Algorithm 2 chooses $n_a = 3$ ancillas for $[[30, 4, 4]]$ BB6 code and $n_a = 6$ for $[[48, 4, 6]]$ BB6 code.

[2] presented a remarkably simple fitting formula

$$p_L = c(p/p_{th})^{(d+1)/2}, \quad (C1)$$

where d is the distance of the code, p_L is the logical error rate, p is the physical error rate, c and p_{th} are constants. For the parallel circuit model, the constants are $c = 0.03$ and $p_{th} = 0.0057$ [2]. Note that the same formula (C1) with the same constants c and p_{th} effectively approximates the logical error rate of all surface codes. In contrast, [47] uses a more complicated formula $p_L = p^{d/2} e^{c_0 + c_1 p + c_2 p^2}$ to fit BB6 codes, and each BB6 code instance requires a distinct set of constants c_0, c_1, c_2 .

Under the ion chain model, we find that the formula (C1) with constants $c = 0.003$ and $p_{th} = 0.0032$ provides a good fit for the 3 surface codes in Table I. However, this formula does not generalize to longer surface codes with distance larger than 7. For BB5 codes, we use a more complicated fitting formula $p_L = p^{(d+1)/2} e^{c_0 + c_1 p + c_2 p^2}$, where each BB5 code instance has its own set of constants c_0, c_1, c_2 . These constants for the two BB5 code instances are listed in Table III.

$[[n, k, d]]$	c_0	c_1	c_2
$[[30, 4, 5]]$	12.869	-340.43	15878
$[[48, 4, 7]]$	18.256	-260.44	680.65

TABLE III. Constants in the fitting formula $p_L = p^{(d+1)/2} e^{c_0 + c_1 p + c_2 p^2}$ for BB5 codes.

-
- [1] E. Dennis, A. Kitaev, A. Landahl, and J. Preskill, Topological quantum memory, *Journal of Mathematical Physics* **43**, 4452 (2002).
 - [2] A. G. Fowler, M. Mariantoni, J. M. Martinis, and A. N. Cleland, Surface codes: Towards practical large-scale quantum computation, *Physical Review A—Atomic, Molecular, and Optical Physics* **86**, 032324 (2012).
 - [3] H. Bombin and M. A. Martin-Delgado, Topological quantum distillation, *Physical review letters* **97**, 180501 (2006).
 - [4] E. H. Chen, T. J. Yoder, Y. Kim, N. Sundaresan, S. Srinivasan, M. Li, A. D. Córcoles, A. W. Cross, and M. Takita, Calibrated decoders for experimental quantum error correction, *Physical Review Letters* **128**, 110504 (2022).
 - [5] S. Krinner, N. Lacroix, A. Remm, A. Di Paolo, E. Genois, C. Leroux, C. Hellings, S. Lazar, F. Swiadek, J. Herrmann, *et al.*, Realizing repeated quantum error correction in a distance-three surface code, *Nature* **605**, 669 (2022).
 - [6] Y. Zhao, Y. Ye, H.-L. Huang, Y. Zhang, D. Wu, H. Guan, Q. Zhu, Z. Wei, T. He, S. Cao, *et al.*, Realization of an error-correcting surface code with superconducting qubits, *Physical Review Letters* **129**, 030501 (2022).
 - [7] Suppressing quantum errors by scaling a surface code logical qubit, *Nature* **614**, 676 (2023).
 - [8] G. Q. Ai *et al.*, Quantum error correction below the surface code threshold, *Nature* **638**, 920 (2024).
 - [9] N. Lacroix, A. Bourassa, F. J. Heras, L. M. Zhang, J. Bausch, A. W. Senior, T. Edlich, N. Shutty, V. Sivak, A. Bengtsson, *et al.*, Scaling and logic in the color code on a superconducting quantum processor, *arXiv preprint arXiv:2412.14256* (2024).
 - [10] R. Chao, M. E. Beverland, N. Delfosse, and J. Haah, Optimization of the surface code design for majorana-based qubits, *Quantum* **4**, 352 (2020).
 - [11] A. Paetznick, C. Knapp, N. Delfosse, B. Bauer, J. Haah,

- M. B. Hastings, and M. P. da Silva, Performance of planar floquet codes with majorana-based qubits, *PRX Quantum* **4**, 010310 (2023).
- [12] D. Bluvstein, S. J. Evered, A. A. Geim, S. H. Li, H. Zhou, T. Manovitz, S. Ebadi, M. Cain, M. Kalinowski, D. Hangleiter, *et al.*, Logical quantum processor based on reconfigurable atom arrays, *Nature* **626**, 58 (2024).
- [13] Q. Xu, J. P. Bonilla Ataides, C. A. Pattison, N. Raveendran, D. Bluvstein, J. Wurtz, B. Vasić, M. D. Lukin, L. Jiang, and H. Zhou, Constant-overhead fault-tolerant quantum computation with reconfigurable atom arrays, *Nature Physics* **20**, 1084 (2024).
- [14] S. Veroni, M. Müller, and G. Giudice, Optimized measurement-free and fault-tolerant quantum error correction for neutral atoms, *Physical Review Research* **6**, 043253 (2024).
- [15] B. W. Reichardt, A. Paetznick, D. Aasen, I. Basov, J. M. Bello-Rivas, P. Bonderson, R. Chao, W. van Dam, M. B. Hastings, A. Paz, *et al.*, Logical computation demonstrated with a neutral atom quantum processor, arXiv preprint arXiv:2411.11822 (2024).
- [16] L. Pecorari, S. Jandura, G. K. Brennen, and G. Pupillo, High-rate quantum ldpc codes for long-range-connected neutral atom registers, *Nature Communications* **16**, 1111 (2025).
- [17] J. Guillaud and M. Mirrahimi, Repetition cat qubits for fault-tolerant quantum computation, *Physical Review X* **9**, 041053 (2019).
- [18] D. Ruiz, J. Guillaud, A. Leverrier, M. Mirrahimi, and C. Vuillot, Ldpc-cat codes for low-overhead quantum computing in 2d, *Nature Communications* **16**, 1040 (2025).
- [19] H. Putterman, K. Noh, C. T. Hann, G. S. MacCabe, S. Aghaeimeibodi, R. N. Patel, M. Lee, W. M. Jones, H. Moradinejad, R. Rodriguez, *et al.*, Hardware-efficient quantum error correction via concatenated bosonic qubits, *Nature* **638**, 927 (2025).
- [20] S. Bartolucci, P. Birchall, H. Bombin, H. Cable, C. Dawson, M. Gimeno-Segovia, E. Johnston, K. Kieling, N. Nickerson, M. Pant, *et al.*, Fusion-based quantum computation, *Nature Communications* **14**, 912 (2023).
- [21] G. de Glinasty, P. Hilaire, P.-E. Emeriau, S. C. Wein, A. Salavrakos, and S. Mansfield, A spin-optical quantum computing architecture, *Quantum* **8**, 1423 (2024).
- [22] P. Hilaire, T. Dessertaine, B. Bourdoncle, A. Denys, G. de Glinasty, G. Valentí-Rojas, and S. Mansfield, Enhanced fault-tolerance in photonic quantum computing: Floquet code outperforms surface code in tailored architecture, arXiv preprint arXiv:2410.07065 (2024).
- [23] B. W. Walshe, B. Q. Baragiola, H. Ferretti, J. Gefaell, M. Vasmer, R. Weil, T. Matsuura, T. Jaeken, G. Pantaleoni, Z. Han, *et al.*, Linear-optical quantum computation with arbitrary error-correcting codes, *Physical Review Letters* **134**, 100602 (2025).
- [24] C. Ryan-Anderson, J. G. Bohnet, K. Lee, D. Gresh, A. Hankin, J. Gaebler, D. Francois, A. Chernoguzov, D. Lucchetti, N. C. Brown, *et al.*, Realization of real-time fault-tolerant quantum error correction, *Physical Review X* **11**, 041058 (2021).
- [25] C. Ryan-Anderson, N. Brown, C. Baldwin, J. Dreiling, C. Foltz, J. Gaebler, T. Gatterman, N. Hewitt, C. Holliman, C. Horst, *et al.*, High-fidelity teleportation of a logical qubit using transversal gates and lattice surgery, *Science* **385**, 1327 (2024).
- [26] A. Paetznick, M. da Silva, C. Ryan-Anderson, J. Bello-Rivas, J. Campora III, A. Chernoguzov, J. Dreiling, C. Foltz, F. Frachon, J. Gaebler, *et al.*, Demonstration of logical qubits and repeated error correction with better-than-physical error rates, arXiv preprint arXiv:2404.02280 (2024).
- [27] T. Monz, D. Nigg, E. A. Martinez, M. F. Brandl, P. Schindler, R. Rines, S. X. Wang, I. L. Chuang, and R. Blatt, Realization of a scalable shor algorithm, *Science* **351**, 1068 (2016).
- [28] S. Debnath, N. M. Linke, C. Figgatt, K. A. Landsman, K. Wright, and C. Monroe, Demonstration of a small programmable quantum computer with atomic qubits, *Nature* **536**, 63 (2016).
- [29] T. Monz, P. Schindler, J. T. Barreiro, M. Chwalla, D. Nigg, W. A. Coish, M. Harlander, W. Hänsel, M. Hennrich, and R. Blatt, 14-qubit entanglement: Creation and coherence, *Physical Review Letters* **106**, 130506 (2011).
- [30] Y. Nam, J.-S. Chen, N. C. Pienti, K. Wright, C. Delaney, D. Maslov, K. R. Brown, S. Allen, J. M. Amini, J. Apisdorf, *et al.*, Ground-state energy estimation of the water molecule on a trapped-ion quantum computer, *npj Quantum Information* **6**, 33 (2020).
- [31] L. Egan, D. M. Debroy, C. Noel, A. Risinger, D. Zhu, D. Biswas, M. Newman, M. Li, K. R. Brown, M. Cetina, *et al.*, Fault-tolerant control of an error-corrected qubit, *Nature* **598**, 281 (2021).
- [32] L. N. Egan, *Scaling quantum computers with long chains of trapped ions*, Ph.D. thesis, University of Maryland, College Park (2021).
- [33] L. Postler, S. Heußen, I. Pogorelov, M. Rispler, T. Feldker, M. Meth, C. D. Marciniak, R. Stricker, M. Ringbauer, R. Blatt, *et al.*, Demonstration of fault-tolerant universal quantum gate operations, *Nature* **605**, 675 (2022).
- [34] J.-S. Chen, E. Nielsen, M. Ebert, V. Inlek, K. Wright, V. Chaplin, A. Maksymov, E. Pérez, A. Poudel, P. Maunz, *et al.*, Benchmarking a trapped-ion quantum computer with 29 algorithmic qubits, arXiv e-prints, arXiv (2023).
- [35] J. Zhang, G. Pagano, P. W. Hess, A. Kyprianidis, P. Becker, H. Kaplan, A. V. Gorshkov, Z.-X. Gong, and C. Monroe, Observation of a many-body dynamical phase transition with a 53-qubit quantum simulator, *Nature* **551**, 601 (2017).
- [36] F. Kranzl, M. K. Joshi, C. Maier, T. Brydges, J. Franke, R. Blatt, and C. F. Roos, Controlling long ion strings for quantum simulation and precision measurements, *Physical Review A* **105**, 052426 (2022).
- [37] M. R. Kamsap, C. Champenois, J. Pedregosa-Gutierrez, S. Mahler, M. Houssin, and M. Knoop, Experimental demonstration of an efficient number diagnostic for long ion chains, *Physical Review A* **95**, 013413 (2017).
- [38] D. Kielpinski, C. Monroe, and D. J. Wineland, Architecture for a large-scale ion-trap quantum computer, *Nature* **417**, 709 (2002).
- [39] C. Monroe, R. Raussendorf, A. Ruthven, K. R. Brown, P. Maunz, L.-M. Duan, and J. Kim, Large-scale modular quantum-computer architecture with atomic memory and photonic interconnects, *Physical Review A* **89**, 022317 (2014).
- [40] D. Schwerdt, L. Peleg, Y. Shapira, N. Priel, Y. Florshaim, A. Gross, A. Zalic, G. Afek, N. Akerman, A. Stern, *et al.*, Scalable architecture for trapped-ion quantum computing using rf traps and dynamic optical potentials, *Phys-*

- ical Review X **14**, 041017 (2024).
- [41] C. D. Bruzewicz, J. Chiaverini, R. McConnell, and J. M. Sage, Trapped-ion quantum computing: Progress and challenges, *Applied physics reviews* **6** (2019).
 - [42] M. DeCross, R. Haghshenas, M. Liu, E. Rinaldi, J. Gray, Y. Alexeev, C. H. Baldwin, J. P. Bartolotta, M. Bohn, E. Chertkov, *et al.*, The computational power of random quantum circuits in arbitrary geometries, *arXiv preprint arXiv:2406.02501* (2024).
 - [43] C. Löschnauer, J. M. Toba, A. Hughes, S. King, M. Weber, R. Srinivas, R. Matt, R. Nourshargh, D. Allcock, C. Ballance, *et al.*, Scalable, high-fidelity all-electronic control of trapped-ion qubits, *arXiv preprint arXiv:2407.07694* (2024).
 - [44] A. Sørensen and K. Mølmer, Quantum computation with ions in thermal motion, *Physical review letters* **82**, 1971 (1999).
 - [45] A. Sørensen and K. Mølmer, Entanglement and quantum computation with ions in thermal motion, *Physical Review A* **62**, 022311 (2000).
 - [46] M. A. Tremblay, N. Delfosse, and M. E. Beverland, Constant-overhead quantum error correction with thin planar connectivity, *Physical Review Letters* **129**, 050504 (2022).
 - [47] S. Bravyi, A. W. Cross, J. M. Gambetta, D. Maslov, P. Rall, and T. J. Yoder, High-threshold and low-overhead fault-tolerant quantum memory, *Nature* **627**, 778 (2024).
 - [48] N. Berthussen, D. Devulapalli, E. Schoute, A. M. Childs, M. J. Gullans, A. V. Gorshkov, and D. Gottesman, Toward a 2d local implementation of quantum low-density parity-check codes, *PRX Quantum* **6**, 010306 (2025).
 - [49] D. Gottesman, *Stabilizer codes and quantum error correction* (California Institute of Technology, 1997).
 - [50] C. Myatt, E. Burt, R. Ghrist, E. A. Cornell, and C. Wieman, Production of two overlapping bose-einstein condensates by sympathetic cooling, *Physical Review Letters* **78**, 586 (1997).
 - [51] A. R. Calderbank and P. W. Shor, Good quantum error-correcting codes exist, *Physical Review A* **54**, 1098 (1996).
 - [52] A. Steane, Multiple-particle interference and quantum error correction, *Proceedings of the Royal Society of London. Series A: Mathematical, Physical and Engineering Sciences* **452**, 2551 (1996).
 - [53] C. Gidney, Stim: a fast stabilizer circuit simulator, *Quantum* **5**, 497 (2021).
 - [54] P. Panteleev and G. Kalachev, Degenerate quantum LDPC codes with good finite length performance, *Quantum* **5**, 585 (2021).
 - [55] J. Roffe, D. R. White, S. Burton, and E. Campbell, Decoding across the quantum low-density parity-check code landscape, *Physical Review Research* **2** (2020).
 - [56] J. Roffe, LDPC: Python tools for low density parity check codes (2022).
 - [57] O. Higgott and C. Gidney, Sparse Blossom: correcting a million errors per core second with minimum-weight matching, *Quantum* **9**, 1600 (2025).
 - [58] T. R. Scruby, T. Hillmann, and J. Roffe, High-threshold, low-overhead and single-shot decodable fault-tolerant quantum memory, *arXiv preprint arXiv:2406.14445* (2024).
 - [59] H.-K. Lin and L. P. Pryadko, Quantum two-block group algebra codes, *Physical Review A* **109**, 022407 (2024).
 - [60] M. Wang and F. Mueller, Coprime bivariate bicycle codes and their properties, *arXiv preprint arXiv:2408.10001* (2024).
 - [61] J. N. Eberhardt, F. R. F. Pereira, and V. Steffan, Pruning qldpc codes: Towards bivariate bicycle codes with open boundary conditions, *arXiv preprint arXiv:2412.04181* (2024).
 - [62] H.-K. Lin, X. Liu, P. K. Lim, and L. P. Pryadko, Single-shot and two-shot decoding with generalized bicycle codes, *arXiv preprint arXiv:2502.19406* (2025).
 - [63] V. Guemard and G. Zémor, Moderate-length lifted quantum tanner codes, *arXiv preprint arXiv:2502.20297* (2025).
 - [64] S. Bravyi and A. Vargo, Simulation of rare events in quantum error correction, *Phys. Rev. A* **88**, 062308 (2013).